

# Experimental Determination of Absolute Spectral Radiance and Emissivity of a Photonic Crystal Filament

Mei-Li Hsieh, A. Kaiser, T. Romero , James A. Bur, Shankar Narayanan , A. Levitan, and Shawn-Yu Lin , *Member, IEEE*

**Abstract**—A recent discovery of super-Planckian radiation in the far-field has attracted a great deal of interest in thermal radiation control using photonic crystals (PC) architecture. The finding is based on a careful comparison of radiation intensity emitted from a PC nano-filament and a blackbody at the same temperature and same wavelength at  $\lambda \sim 1.7 \mu\text{m}$ . Extending that finding, we determined the absolute spectral radiance of such a PC filament at  $\lambda \sim 1.7 \mu\text{m}$  at elevated temperature,  $T = 445\text{--}723 \text{ K}$ , and compared its value to that predicted by Planck's blackbody radiation law. Our data confirmed that the PC spectral radiance surpassed that of a blackbody by an order-of-magnitude. We also determined the spectral emissivity of our PC filament and showed that its value far exceeded unity at resonance and fell below unity away from resonance. The observation of non-equality between absorptivity and emissivity suggests that a strong optical non-reciprocity takes place in our PC nano-filament.

**Index Terms**—Nano-photonics, novel photon sources, photonic crystals, photonic materials and engineered photonic structures.

## I. INTRODUCTION

THE concept of a three-dimensional photonic-crystal (PC) was first introduced in 1987 [1], [2] for light-trapping [3], [4], [5], diffractionless waveguiding [6], [7] and strong modification of spontaneous [2] and thermal emission [8]. The first realization of an all-metallic PC was accomplished in 2002. An exceedingly large photonic band gap in the infrared was shown. Hence, a metallic PC provides ideal for thermal radiation control over a broad wavelength range [9]. Upon thermal excitation, a metallic PC [10], [11], [12] exhibits radiation spectra distinctly different from that of an ideal blackbody [13], having radiation peaks corresponding to the features of the underlying PC. Furthermore, the peak radiation intensity can exceed that

of a blackbody under the same experimental conditions, i.e., super-Planckian behavior [14]. The finding is based on a careful comparison of radiation intensity emitted from a PC and a blackbody at the same temperature, wavelength and in the far field. Up until now, there was no experimental determination of the absolute spectral radiance of a PC. Nor could it be compared to the radiance theoretically predicted by Planck's blackbody radiation law.

## II. FINDINGS

In this work, we measured the absolute spectral radiance of a tungsten, 3D PC (now called W-PC) and compared it to the ideal blackbody spectral radiance. The experiment was done by first coating half of the W-PC sample with a layer of carbon-nanotube (CNT) having 99.9% absorptance [15], which serves as the blackbody reference. Under thermal excitation, the blackbody emission spectrum gives an accurate determination of sample's surface temperature by curve fitting to the Planck's blackbody spectrum curve. Secondly, the PC emission spectrum and absolute power was measured from the uncoated region of the sample over the resonance regime ( $\lambda = 1550\text{--}1750\text{nm}$ ). From these two measurements, we determined the absolute spectral radiance of a PC sample and demonstrated that it surpassed that of a blackbody by an order-of-magnitude.

The sample we used in this experiment consisted of a micro-cavity fabricated on top of a 3D W-PC on a four-inch silicon wafer. The role of the cavity is to enhance optical resonance and to reduce the emission linewidth, thus forming a passband for PC light emission to channel out to free space [16]. The micro-cavity was formed by a  $\text{SiO}_2$  layer of thickness  $t_{\text{cav}} = 554 \text{ nm}$  sandwiched on both sides by  $\text{SiO}_2/\text{Si}$  Distributed Bragg Reflector (DBR) mirrors. The thicknesses of the  $\text{SiO}_2$  and Si are  $t_{\text{oxide}} = 275$  and  $t_{\text{Si}} = 120 \text{ nm}$ , respectively. The 3D W-PC had diamond lattice symmetry [17] and consisted of six layers of alternating one-dimensional tungsten-rods [9], [10]. The 1D tungsten-rods had a height of  $h = 0.6 \mu\text{m}$ , a rod width of  $w = 0.5 \mu\text{m}$  and a rod-to-rod spacing of  $a = 1.5 \mu\text{m}$ . Before thermal testing, the PC-cavity sample area was  $\sim 7 \times 7 \text{ mm}^2$  and the silicon substrate was thinned down to  $\sim 300 \mu\text{m}$  for mounting purposes.

Fig. 1(a) shows a photo of our W-PC sample setting up procedure. The left-side of the sample was coated with a layer of

Manuscript received 13 July 2022; revised 2 October 2022; accepted 9 October 2022. Date of publication 12 October 2022; date of current version 21 October 2022. This work was supported by the Defense Advanced Research Projects Agency (DARPA) under Grant HR001121C0147. (Corresponding author: Shawn-Yu Lin.)

Mei-Li Hsieh, A. Kaiser, T. Romero, James A. Bur, and Shawn-Yu Lin are with the Department of Physics, Applied Physics and Astronomy, Rensselaer Polytechnic Institute, Troy, NY 12180 USA (e-mail: hsiehm@rpi.edu; kaisea2@rpi.edu; romert@rpi.edu; burj@rpi.edu; sylin@rpi.edu).

Shankar Narayanan is with the Department of Mechanical, Aerospace and Nuclear Engineering, Rensselaer Polytechnic Institute, Troy, NY 12180 USA (e-mail: narays5@rpi.edu).

A. Levitan is with the PSquaredT LLC, Wilton, CT 06897 USA (e-mail: ppt.arthur@snet.net).

Digital Object Identifier 10.1109/JPHOT.2022.3213988

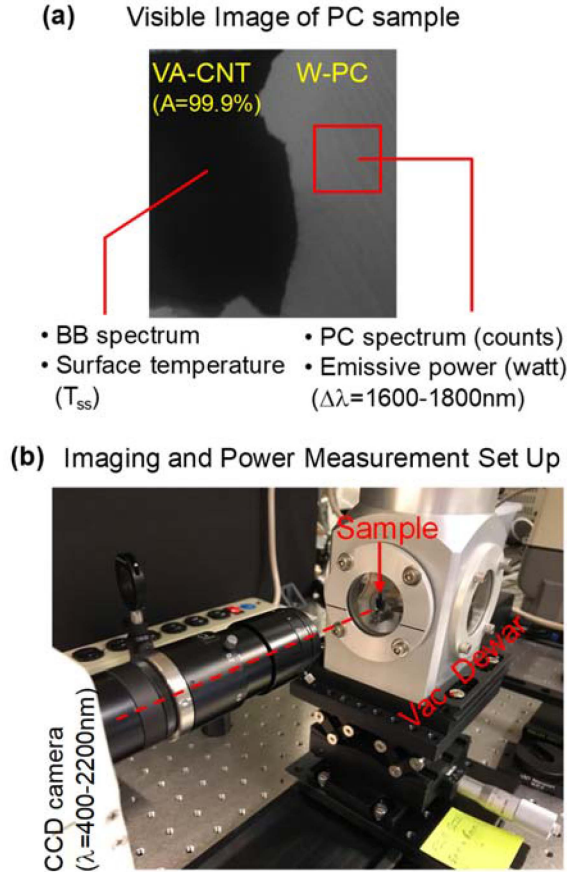


Fig. 1. The photonic-crystal sample and the emission testing setup. (a) The left-side of the  $7 \times 7 \text{ mm}^2$  tungsten-photonic-crystal (W-PC) sample is coated with a layer of black carbon-nanotube material (CNT), which serves as the black reference. (b) The experimental setup. The W-PC sample is placed inside a high vacuum Dewar, pumped to  $1 \times 10^{-7}$  torr to eliminate convection loss. A FTIR (Fourier Infrared Spectrometer) is used to measure CNT and W-PC emission spectrum in the infrared. A calibrated Newport power meter, in combination with a bandpass filter, is used to measure optical power emitted from the W-PC over the  $\lambda = 1550\text{--}1750 \text{ nm}$  peak emission band.

vertically-aligned-carbon-nanotube material (VA-CNT), which served as the blackbody reference [15], [18]. It is noted that the absorptance of our VA-CNT sample has a weak angular dependence [15], and may be regarded as a near isotropic material. The uneven vertical boundary near the center was caused by non-ideal peeling of the VA-CNT material from its original substrate. Also, for the purpose of thermal heating, the W-PC sample was mounted on top of an electrically driven heater by the use of a  $\sim 300 \mu\text{m}$  thick thermally conductive blackbody paint [19]. Fig. 1(b) shows a photo of high vacuum optical Dewar. Since the sample was to be heated to elevated temperatures,  $T = 400\text{--}750 \text{ }^\circ\text{K}$ , it was placed inside the Dewar to minimize thermal convection loss. When the PC sample is heated, it emits radiation through the infrared transparent optical salt window and is detected either by a spectrometer, an infrared CCD camera or an optical power meter. The emission pattern is directional with an angular spread of 20 degrees and the emission optical axis is indicated as the horizontal red dotted line. Note that, in our experimental configuration, the lattice temperature of the

blackbody and the PC regions, were shown to be identical to within  $\Delta T = 0.1 \text{ K}$  across the PC/CNT boundary and  $\Delta T < 5\text{K}$  across the entire sample [20].

In the following, we describe the sample's optical testing procedure. In step-(1), a FTIR (Fourier-Transform-Infrared-Spectrometer) is used to measure CNT radiation spectrum in the infrared,  $\lambda = 2\text{--}20 \mu\text{m}$ , at a series of heater biased currents. The measured spectrum is then fitted to the standard blackbody radiation curve to obtain the sample's surface temperature at each biased current. In step-(2), the FTIR is also used to measure PC-radiation spectrum (the right-hand side of the sample indicated by the red square of  $3 \times 4 \text{ mm}^2$ ), but in the near-infrared regime,  $\lambda = 1.2\text{--}3.5 \mu\text{m}$ . This process is intended to measure the primary PC-emission peak at  $\lambda \sim 1.7 \mu\text{m}$  regime. In step-(3), a calibrated Newport power meter (Model 843-R) with Newport Power head (Model 918-ST-IR) is used to measure the PC-radiative power emitted from the red square region over  $\lambda = 1550\text{--}1750 \text{ nm}$ . A bandpass filter is placed in front of the power meter to ensure that only radiation power over  $\lambda = 1550\text{--}1750 \text{ nm}$  is measured. Using the spectral and power data obtained from steps-(2) and -(3), the absolute spectral radiance of PC-radiation can be determined.

Fig. 2(a) shows the measured radiation spectra of the black CNT portion of the sample (the black curves) taken at a series of heater biased current,  $I = 2.0\text{--}3.8 \text{ A}$ . The emissive power is detected by a DTGS detector and is expressed in a relative unit, "counts". The measured radiation curve  $f(\lambda, T)$  is then fitted to the standard blackbody radiation curve  $M_e$  [21]:

$$f(\lambda, T) = M_e(\lambda, T) \times \alpha = \left[ 40720 \times \frac{1}{\lambda^5} \times \frac{1}{e^{(14404/\lambda T)} - 1} \right] \times \alpha \quad (1)$$

Here,  $\alpha$  and  $T$  are two fitting parameters and  $\lambda$  and  $T$  are expressed in  $\mu\text{m}$  and K, respectively. The parameter " $\alpha$ " is a conversion factor between the emitted CNT radiation and the detected signal count by the FTIR photo-detector. Because the CNT material is not an ideal blackbody over the entire infrared ( $\lambda = 2\text{--}20 \mu\text{m}$ ), we fitted the measured curves only in the mid-infrared regime ( $\lambda = 2\text{--}8 \mu\text{m}$ ). Fig. 2(b) shows the result of that curve fitting. Five representative measured data are shown as the colored curves and the corresponding fitted curves are the black curves. The measured and fitted curves show good agreement over  $\lambda = 3.5\text{--}6.5 \mu\text{m}$ , where the peak radiation wavelength occurs. From the juxtaposition of these curves, the sample's surface temperature is determined to be  $T = 683.9, 661, 633.7, 603.3$  and  $569.1 \text{ }^\circ\text{K}$  for  $I = 3.4, 3.2, 3.0, 2.8$  and  $2.6\text{A}$ , respectively [22]. Note that, for all the fitting curves, we were able to use a single value of  $\alpha = 1.40$  to obtain a good fit at all temperatures. This is a reasonable approach because  $\alpha$  in equation-(1) should depend only on the detector's photo-response and should be temperature-independent. However, the procedure does cause a slightly higher CNT emissive power than the theoretical blackbody power at  $\lambda = 2\text{--}3 \mu\text{m}$  regime and a slightly lower CNT emissive power than the blackbody's at  $\lambda = 7\text{--}8 \mu\text{m}$  regime. Nonetheless, the overall fit is still good. Using

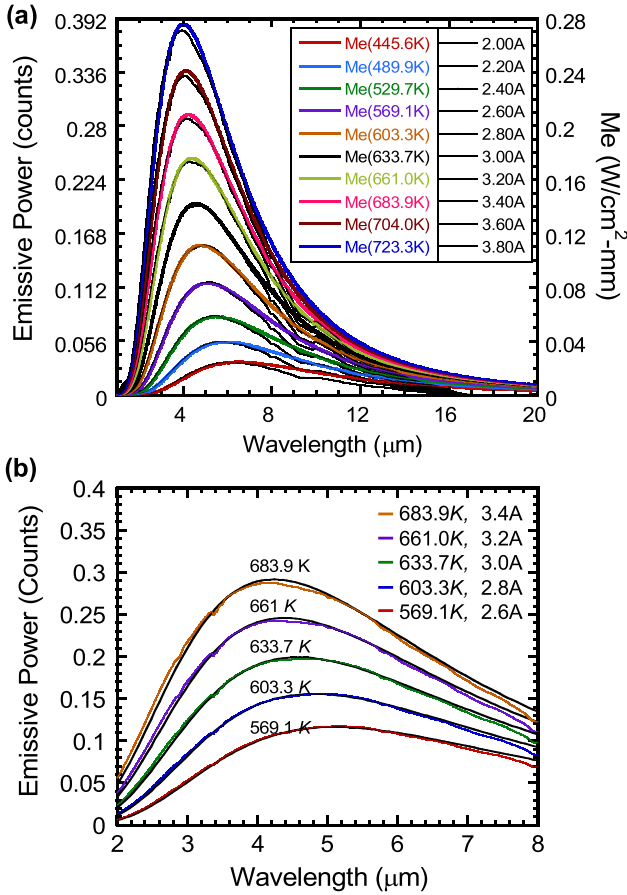


Fig. 2. Accurate determination of sample's surface temperature. (a) shows the black CNT portion of the sample (the black curves) infrared radiation spectra over  $\lambda = 2\text{--}20\ \mu\text{m}$  and for a series of heater bias current,  $I = 2.0\text{--}3.8\ \text{A}$ . The emissive power is detected by an infrared DTGS photodetector and is expressed in a relative unit, "counts". The observed radiation curves are fitted to the standard blackbody radiation curves  $M_e(\lambda, T)$  (the colored curves). Here  $\alpha$  and  $T$  are the two curve fitting parameters. Since CNT is not an ideal blackbody over  $\lambda = 2\text{--}20\ \mu\text{m}$ , we fit the measured curves only in the mid-infrared  $\lambda = 2\text{--}8\ \mu\text{m}$  regime. (b) shows the result of the fitting to the blackbody radiation curves. Five representative measured curves are shown as the black curves and the corresponding fitted blackbody curves as the colored curves. The fits show good agreement and yield a sample's surface temperature of  $T = 683.9, 661.0, 633.7, 603.3$  and  $569.1\ \text{K}$  for  $I = 3.4, 3.2, 3.0, 2.8$  and  $2.6\ \text{A}$ , respectively.

the obtained  $\alpha$  and  $T_s$ , the fitted blackbody radiation spectra are shown in Fig. 2(a) as the color curves over  $\lambda = 2\text{--}20\ \mu\text{m}$ . This time, the right-hand-side vertical axis has a unit of spectral radiance  $[\text{W}/\text{cm}^2\text{-}\mu\text{m}]$ .

These curve fitting results show that our CNT material is a nearly ideal blackbody over  $\lambda = 3\text{--}6.5\ \mu\text{m}$ . Hence, its radiation spectrum can yield an accurate surface temperature of our heated sample at a given biased current. For  $\lambda > 8\ \mu\text{m}$ , the CNT radiation starts to deviate from the standard blackbody spectrum. This point will be addressed in a later paragraph.

Next, we report the spectral radiance of our PC sample in the near-infrared regime,  $\lambda = 1\text{--}2.5\ \mu\text{m}$ , at  $I = 2.0\text{--}3.8\ \text{A}$  or  $T = 445.6\text{--}723.3\ \text{K}$ . Fig. 3 shows the measured spectral radiance v.s.  $\lambda$  (the black curves) for our PC sample at five different  $T = 603.3\text{--}723.3\ \text{K}$ . As described earlier, the spectral radiance is obtained by a combination of spectroscopic measurement using FTIR and a calibrated optical power meter over  $\lambda = 1550\text{--}1750$

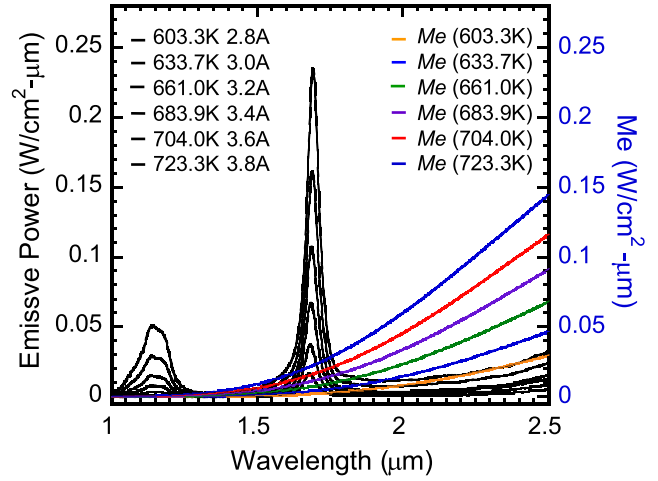


Fig. 3. Determination of spectral radiance of W-PC at elevated temperatures. The measured emissive power has a radiance unit of  $(\text{W}/\text{cm}^2\text{-}\mu\text{m})$  and is plotted vs. wavelength ( $\lambda = 1\text{--}2.5\ \mu\text{m}$ ) for sample at different temperatures  $T = 603.3\text{--}723.3\ \text{K}$ . It is obtained by a combination of FTIR spectroscopic measurement and power measurement over  $\lambda = 1550\text{--}1750\text{nm}$ . As a comparison, we also show the standard blackbody spectral radiance ( $M_e$ ) curve at the same  $T$  from  $603.3\text{--}723.3\ \text{K}$ . Although similar comparisons have been made before, this data represents the first direct comparison of absolute spectral radiance between a heated W-PC and an ideal blackbody.

nm. The emission peak at  $\lambda \sim 1.7\ \mu\text{m}$  is due to the fundamental passband resonance of the DBR cavity [16]. The peak spectral radiance increases from  $0.017$  to  $0.24\ \text{W}/\text{cm}^2\text{-}\mu\text{m}$  when  $T$  is increased from  $603.3\ \text{K}$  to  $723.3\ \text{K}$ . As a comparison, in Fig. 3 we show the standard blackbody spectral radiance ( $M_e$ ) curve (colored curves) computed at the same  $T$  from  $603.3\ \text{K}$  to  $723.3\ \text{K}$ . This comparison confirms that the PC spectral radiance exceeds the blackbody spectral radiance at  $\lambda \sim 1.7\ \mu\text{m}$  for all  $T_s$  tested and shows the super-Planckian behavior in the far-field. Although a similar comparison had been reported earlier [16], this data represents the first direct comparison of absolute spectral radiance between a heated PC sample and what is theoretically expected for an ideal blackbody.

In the following, we discuss optical non-reciprocity taking place in our heated W-PC sample in the  $\lambda = 1.3\text{--}3.5\ \mu\text{m}$  wavelength range. Fig. 4(a) shows the measured reflectance spectrum of a W-PC sample taken at room temperature,  $T \sim 300\ \text{K}$ , and at normal incidence. The two reflectance dips at  $\lambda \sim 1.7\ \mu\text{m}$  and  $2.85\ \mu\text{m}$  correspond to the fundamental resonance and band edge resonance of the DBR/W-PC structure, respectively.

Fig. 4(b) shows the absorptance spectrum of the sample also at room temperature and normal incidence, where  $A(\lambda) = 1 - R(\lambda)$ . The absorptance is found to be  $\alpha_1 = 0.90$  and  $\alpha_2 = 0.80$  for the  $\lambda \sim 1.7\ \mu\text{m}$  and  $2.85\ \mu\text{m}$  resonances, respectively. It is noted that the PC has a near-unity absorptivity ( $\alpha_1 = 0.9$ ) at  $\lambda \cong 1.7\ \mu\text{m}$  at room temperature, any increase of its value due to an increased temperature would not change too much of its absorptivity. Fig. 4(c) shows the spectral emissivity,  $\varepsilon(\lambda)$ , of the W-PC sample measured at elevated temperatures,  $T = 603.3\text{--}723.3\ \text{K}$ . The spectral emissivity is defined as the ratio of PC radiation to the theoretical blackbody radiation at the



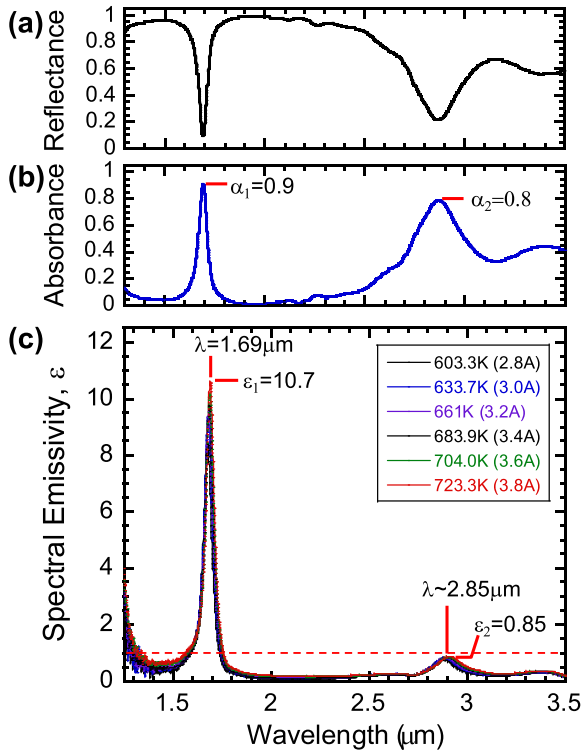
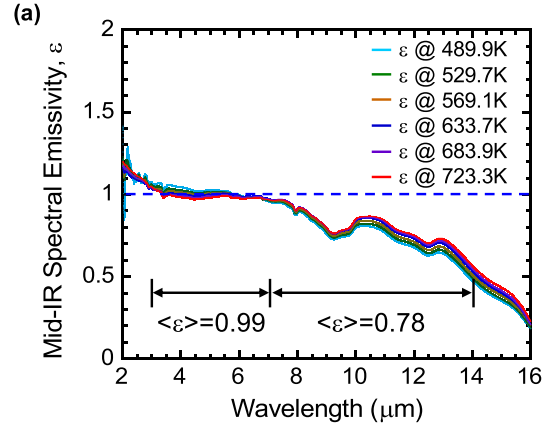


Fig. 4. Demonstration of optical non-reciprocity in a heated W-PC sample. (a) shows the reflectance spectrum of our PC sample at room temperature,  $T = 300$  K, and normal incidence. The two reflectance dips at  $\lambda = 1.7$  and  $\lambda \sim 2.85$   $\mu\text{m}$  correspond to the fundamental resonance and band edge resonance of the DBR/W-PC structure. (b) shows the corresponding absorbance spectrum, where  $\alpha(\lambda) = 1 - R(\lambda)$ . The absorbance is found to be  $\alpha_1 = 0.90$  and  $\alpha_2 = 0.80$  for  $\lambda = 1.7$  and  $\lambda \sim 2.85$   $\mu\text{m}$  resonances, respectively. (c) shows the spectral emissivity,  $\varepsilon(\lambda, T)$ , of our W-PC sample measured at elevated temperatures  $T = 603.3$ – $723.3$  K. The spectral emissivity is defined as the ratio of PC and blackbody spectral radiance at the same temperature,  $\varepsilon(\lambda, T) = PC(\lambda, T)/M_e(\lambda, T)$ . In the fundamental resonance regime, W-PC spectral emissivity is  $\varepsilon_1 = 10.7$  at  $\lambda = 1.7$   $\mu\text{m}$ , which is an order-of-magnitude higher than unity emissivity. Note that its spectral absorbance is  $\alpha_1 = 0.90 < 1.0$ . This data suggests that reciprocity does not hold true in our heated W-PC sample in the resonance regime,  $\lambda \sim 1.7$   $\mu\text{m}$ . This finding further suggests that our heated W-PC can not be under strictly thermal equilibrium condition.

same temperature,  $\varepsilon(\lambda, T) \equiv \frac{PC(\lambda, T)}{M_e(\lambda, T)}$ . The horizontal dashed line indicates unity emissivity, i.e.,  $\varepsilon(\lambda, T) = 1$ .

In the cavity resonance regime, the PC spectral emissivity is  $\varepsilon_1 = 10.7$  at  $\lambda \sim 1.7$   $\mu\text{m}$ , which is an order-of-magnitude above unity emissivity. Away from the cavity resonance, the PC spectral emissivity is  $\varepsilon < 0.2$  and is below unity emissivity. At  $\lambda \sim 2.85$   $\mu\text{m}$ , the PC spectral emissivity is  $\varepsilon \sim 0.85$  and is also below unity emissivity. Additionally, in this temperature range, the PC spectral emissivity only has a weak T-dependence. When we compared to the absorbance values shown in Fig. 4(b), we found  $\varepsilon_1(\lambda = 1.7$   $\mu\text{m}) \gg \alpha_1(\lambda = 1.7$   $\mu\text{m})$  and  $\varepsilon_2(\lambda = 2.85$   $\mu\text{m}) \approx \alpha_2(\lambda = 2.85$   $\mu\text{m})$ . Noted that, in thermal equilibrium and by Kirchhoff's law [23], a hot object's emissivity must be equal to its absorbance so that optical reciprocity holds true. Our data shows that reciprocity is no longer valid for our PC sample in the cavity resonance regime and, hence, demonstrates optical non-reciprocity. This experimental finding further indicates that our W-PC sample might not be under strictly thermal equilibrium [24] under a moderate thermal heating.



(b)

$I_{\text{bias}}$ (A)	$T_{\text{BB}}$ ( $\lambda = 2$ – $8$ $\mu\text{m}$ )	$\langle T \rangle_{\text{ave.}}$ on CNT ( $\varepsilon = 0.95$ )	$\langle T \rangle_{\text{ave.}}$ on CNT ( $\varepsilon = 0.9$ )	$\langle T \rangle_{\text{ave.}}$ on CNT ( $\varepsilon = 0.78$ )
2.0	445.6	403.15	407.65	422.05
2.2	489.9	440.05	445.75	461.95
2.4	529.7	478.05	485.05	504.85
2.6	569.1	514.45	522.75	545.75
2.8	603.3	549.25	558.55	584.85
3.0	633.7	578.35	588.65	617.45
3.2	661	602.55	613.65	644.55
3.4	683.9	624.55	636.35	669.15
3.6	704	644.95	657.25	691.85
3.8	723	665.55	678.55	714.95

Fig. 5. Independent determination of sample's surface temperature by an IR camera. (a) Our infrared camera first measures light emission over  $\lambda = 7$ – $14$   $\mu\text{m}$  from the sample. It then assumes a sample's emissivity  $\varepsilon(\lambda, T)$  and provides the sample's surface temperature reading. The spectral emissivity of our CNT material has been obtained earlier and is plotted vs. wavelength,  $\lambda = 2$ – $16$   $\mu\text{m}$ , for a series of  $T$ s. Here, the spectral emissivity is defined as  $\varepsilon(\lambda, T) = \text{CNT}(\lambda, T)/M_e(\lambda, T)$ , i.e., the ratio of CNT and ideal blackbody spectral radiance given in Fig. 2(a). We find the average emissivity over  $\lambda = 7$ – $14$   $\mu\text{m}$  to be  $\langle \varepsilon \rangle = 0.78$ . (b) is a table summarizing the sample's surface temperature determined by least-square fitting to black CNT over  $\lambda = 2$ – $8$   $\mu\text{m}$  and also from the IR camera reading assuming a CNT's emissivity of  $\langle \varepsilon \rangle = 0.95$ ,  $0.90$  and  $0.78$ . We found that, as long as we use the experimentally determined average emissivity of  $\langle \varepsilon \rangle = 0.78$ , the two methods of temperature measurement agree with each other within  $\Delta T = 10$ – $25$  K.

The validity of our experimental finding of super-Planckian behavior and optical reciprocity depends critically on an accurate measurement of sample's surface temperature. An independent determination of sample's temperature was conducted using a commercially available infrared camera, FLIR camera, Model A655sc [25]. The infrared camera detects light emission from the sample, assumes a spectral emissivity over  $\lambda = 7$ – $14$   $\mu\text{m}$  and yields the sample's surface temperature. Fig. 5(a) show infrared spectral emissivity  $\varepsilon(\lambda, T)$  of the CNT material at a series of  $T$ s for  $\lambda = 2$ – $16$   $\mu\text{m}$ . Here, the spectral emissivity is defined as  $\varepsilon(\lambda, T) = \frac{\text{CNT}(\lambda, T)}{M_e(\lambda, T)}$ , i.e., the ratio of the CNT and ideal blackbody spectral radiance obtained from Fig. 2(a). First, the emissivity is slightly higher than unity for  $\lambda = 2$ – $3$   $\mu\text{m}$ . This is due, in part, to the choice of a single “ $\alpha$ ” value to perform our least-square-fitting for data of all the  $T$ s studied. Second, the

emissivity is close to unity for  $\lambda = 3\text{--}7\ \mu\text{m}$  and has an average value of  $\langle \varepsilon \rangle = 0.99$ . This is the spectral regime where the CNT material is a nearly ideal blackbody. As a result, we were able to obtain a good fit of CNT radiation spectra to the ideal blackbody curves as shown in Fig. 2(b). Lastly, the emissivity drops steadily from  $\varepsilon \sim 1$  to  $\varepsilon \sim 0.2$  for  $\lambda = 7\text{--}16\ \mu\text{m}$ . Note that the average emissivity over  $\lambda = 7\text{--}14\ \mu\text{m}$  is  $\langle \varepsilon \rangle = 0.78$ . This is the emissivity value we used as an input parameter to the FLIR camera.

Fig. 5(b) summarizes the sample's surface temperatures measurements as determined from the least-square fit to blackbody curves over  $\lambda = 2\text{--}8\ \mu\text{m}$  ( $T_{\text{BB}}$ ) and also from FLIR camera reading ( $\langle T \rangle_{\text{ave.}}$ ) using a CNT average emissivity of  $\langle \varepsilon \rangle = 0.95, 0.90$  and  $0.78$ . Note that for a given, detected power by the FLIR camera, a higher  $\langle \varepsilon \rangle$  value would lead to a lower sample temperature. For instance, at  $I_{\text{bias}} = 2.0\text{A}$ , we find  $T_{\text{BB}} = 445.6^\circ\text{K}$  and  $\langle T \rangle_{\text{ave.}} = 403.15, 407.65$  and  $422.05^\circ\text{K}$  for  $\langle \varepsilon \rangle = 0.95, 0.90$  and  $0.78$ , respectively. The discrepancy between  $T_{\text{BB}}$  and  $\langle T(\varepsilon = 0.78) \rangle_{\text{ave.}}$  is  $\Delta T = 445.6\text{--}422.05 = 23.55\ \text{K}$ . Similarly, at  $I_{\text{bias}} = 3.8\text{A}$ , we find  $T_{\text{BB}} = 723\ \text{K}$  and  $\langle T \rangle_{\text{ave.}} = 665.55, 678.55$  and  $714.95\ \text{K}$  for  $\langle \varepsilon \rangle = 0.95, 0.90$  and  $0.78$ , respectively. And the discrepancy between  $T_{\text{BB}}$  and  $\langle T(\varepsilon = 0.78) \rangle_{\text{ave.}}$  is  $\Delta T = 723\text{--}714.95 = 8.05\ \text{K}$ . Therefore, this comparison shows that, as long as we use the experimentally determined average emissivity  $\varepsilon = 0.78$ , the agreement of temperature measurements between that obtained from the blackbody least-squares fit and the IR camera method is within  $\Delta T = 8\text{--}23.55\ \text{K}$ .

### III. CONCLUSION

We have made a direct determination of the absolute spectral radiance of a tungsten PC and compared it to the ideal blackbody spectral radiance at a series of temperatures. The sample temperature is obtained from a least-square-fit of the CNT radiation spectrum to the ideal blackbody curve. Our data shows that, in the cavity resonance regime of  $\lambda \sim 1.7\ \mu\text{m}$ , PC spectral radiance exceeds that of a blackbody by an order-of-magnitude for  $T = 603.3\text{--}723.3\ \text{K}$ . We further demonstrated that optical non-reciprocity exists in our heated PC in the cavity resonance regime.

### ACKNOWLEDGMENT

Any opinions, findings and conclusions or recommendations expressed in this material are those of the author(s) and do not necessarily reflect the views of the Defense Advanced Research Projects Agency (DARPA).

### REFERENCES

- [1] S. John, "Strong localization of photons in certain disordered dielectric superlattices," *Phys. Rev. Lett.*, vol. 58, 1987, Art. no. 2486.
- [2] E. Yabonovitch, "Inhibited spontaneous emission in solid-state physics and electronics," *Phys. Rev. Lett.*, vol. 58, 1987, Art. no. 2059.

- [3] S. Y. Lin et al., "A three-dimensional photonic crystal operating at infrared wavelengths," *Nature*, vol. 394, pp. 251–253, 1998.
- [4] S. Y. Lin, J. G. Fleming, M. M. Sigalas, R. Biswas, and K. M. Ho, "Photonic band gap micro-cavities in three-dimensions," *Phys. Rev.*, vol. B59, no. R15, 1999, Art. no. R15579.
- [5] B. Frey, P. Kuang, M.-L. Hsieh, J.-H. Jiang, S. John, and S. Y. Lin, "Effectively infinite optical pathlength created by simple-cubic photonic crystal for extreme light trapping," *Sci. Rep.*, vol. 7, 2017, Art. no. 4171.
- [6] S. Y. Lin, E. Chow, V. Hietala, P. R. Villeneuve, and J. D. Joannopoulos, "Experimental demonstration of guiding and bending of electromagnetic waves in a photonic crystal," *Science*, vol. 282, pp. 274–276, 1998.
- [7] A. Chutinan, S. John, and O. Toader, "Diffractionless flow of light in all-optical microchips," *Phys. Rev. Lett.*, vol. 90, 2003, Art. no. 123901.
- [8] S. Y. Lin, J. G. Fleming, E. Chow, J. Bur, K. K. Choi, and A. Goldberg, "Enhancement and suppression of thermal emission by a 3D photonic crystal," *Phys. Rev.*, vol. 62, 2000, Art. no. R2243.
- [9] J. G. Fleming, S. Y. Lin, I. El-Kady, R. Biswas, and K. M. Ho, "All-metallic 3D photonic crystals with a large photonic band-gap," *Nature*, vol. 417, pp. 52–55, 2002.
- [10] S. Y. Lin, J. Moreno, and J. G. Fleming, "Three-dimensional photonic-crystal emitter for thermal photovoltaic power generation," *Appl. Phys. Lett.*, vol. 83, pp. 380–382, 2003.
- [11] S. Y. Lin, J. G. Fleming, and I. El-Kady, "Experimental observation of photonic-crystal emission near a photonic band edge," *Appl. Phys. Lett.*, vol. 83, 2003, Art. no. 593.
- [12] M.-Li Hsieh, J. A. Bur, Q. Du, S. John, and S.-Yu Lin, "Probing the intrinsic optical Bloch-mode emission from a 3D photonic crystal," *Nanotechnology*, vol. 27, 2016, Art. no. 415204.
- [13] M. Planck, *The Theory of Heat Radiation*. New York, NY, USA: Dover Publication, 1959.
- [14] M.-Li Hsieh, S.-Yu Lin, J. A. Bur, and R. Sheno, "Experimental observation of anomalous thermal radiation from a three-dimensional metallic photonic crystal," *Nanotechnology*, vol. 26, 2015, Art. no. 234002.
- [15] Z.-P. Yang, L. Ci, J. A. Bur, S.-Yu Lin, and P. M. Ajayan, "A vertically aligned carbon nanotube array: The darkest manmade material," *Nano Lett.*, vol. 8, 2008, Art. no. 446.
- [16] S.-Yu Lin et al., "An in-situ and direct confirmation of super-planckian thermal radiation emitted from a metallic photonic-crystal at optical wavelengths," *Sci. Rep.*, vol. 10, 2020, Art. no. 5209.
- [17] K. M. Ho, C. T. Chan, C. M. Soukoulis, R. Biswas, and M. Sigalas, "Photonic band gaps in three dimensions: New layer-by-layer periodic structures," *Solid State Commun.*, vol. 89, pp. 413–416, 1994.
- [18] Z.-P. Yang et al., "Experimental observation of extremely weak optical scattering from an interlocking carbon nanotube array," *Appl. Opt.*, vol. 50, pp. 1850–1855, 2011.
- [19] *The Blackbody Paint Used in This Experiment is a High Temperature, T = 300-1600 K, ZYP Zirconium Oxide Paint. The Material is Electrically Insulated and Thermally Conductive*. Manufactured by ZYP Coatings, Tennessee, USA. [Online]. Available: <https://www.sypcoatings.com>
- [20] M.-Li Hsieh et al., "Super planckian thermal radiation emitted from a nanoflament of photonic crystal : A direct imaging study," *IEEE Photon. J.*, vol. 11, no. 6, Dec. 2019, Art. no. 4501408.
- [21] E. L. Dereniak and G. D. Boreman, *Infrared Detectors and Systems*. New York, NY, USA: Wiley, 1996.
- [22] *An Alternative Way to Determine a Sample's T is to Measure its Total Radiative Power Q and Deduce T From the Stefan-Boltzmann law [21]: Q = \sigma \cdot T^4. However, When a Sample is Under Heating by a Thermal Heater, a Broadband Power Meter Collects Not Only CNT Radiance, But Also Background Heating From the Thermal Heater. So, For Practical Consideration, We Chose To Use the Fitting Method To Extract Sample's Lattice Sample*.
- [23] G. Kirchhoff, *Philos. Mag. Ser.*, vol. 4, no. 20, pp. 1–21, 1860.
- [24] S. John and R. Wang, "Metallic photonic-band-gap filament architectures for optimized incandescent lighting," *Phys. Rev. A*, vol. 78, 2008, Art. no. 043809.
- [25] FLIR camera, Model A655sc, 640x480 pixels, IR range: 7.0mm - 15mm, Temperature range: 273.15~932.15 °K, [Online]. Available: <https://www.flir.com/products/a655sc/>